Journal of ELECTRONIC MATERIALS, Vol. 47, No. 9, 2018
https://doi.org/10.1007/s11664-018-6455-7

Enhanced Microwave Absorption Properties of Manganese Dioxide/Carbon Fiber Hybrid with Polyaniline in the X Band

JIN WANG,[1] BO CHENG,[2] HUA QIU,[1,3] and SHUHUA QI[1]

1.—Shaanxi Key Laboratory of Macromolecular Science and Technology, Department of Applied Chemistry, School of Science, Northwestern Polytechnical University, Xi'an 710072, Shaanxi, People's Republic of China. 2.—School of Materials Science and Engineering, Henan University of Technology, Zhengzhou 450001, China. 3.—e-mail: hqiu83@163.com

Uniform PANI/MnO_2/CF hybrids with superior microwave absorption properties were rapidly fabricated via a two-step reaction involving the hydrothermal method and *in situ* polymerization. The morphology and structure of the samples were investigated via scanning electron microscopy, x-ray photoelectron spectroscopy, x-ray powder diffraction and Fourier transform infrared spectroscopy. The nano-size MnO_2 particles grown on the surface of the carbon fiber and the MnO_2/CF were found to be uniformly coated with PANI. Based on TG analysis, the thermal stability of PANI/CF and PANI/MnO_2/CF was superior to that of PANI. According to the results of vector network analysis, the microwave-absorbing capacity of PANI/MnO_2/CF was greater than that of PANI and PANI/CF, and its minimum loss value reached − 22 dB at 10.2 GHz. When the frequency was between 8.7 GHz and 11.7 GHz, the R_L values of the hybrid were less than − 10 dB, which implies that its effective absorption bandwidth is 3.0 GHz in the X band.

Key words: Hydrothermal method, manganese dioxide, microwave absorption, carbon fiber

INTRODUCTION

With the rapid development of science and technology, humanity relies heavily on high-technology systems based on microwave radiation phenomena. Consequently, the rapid development of high-frequency application devices causes serious electromagnetic interference (EMI) pollution. Hence, microwave absorbers that can effectively reduce the reflection of microwave have garnered interest for use in different applications. Materials capable of absorbing electromagnetic signals are also widely applied in industrial, commercial and military fields.[1–3] Therefore, more and more researchers are engaged in the exploitation of novel microwave-absorbing materials. A superior material for microwave absorption should be thin and exhibit low density, broad effective absorption frequency, and strong absorption peaks along with other advantageous properties.[4–6] In order to fabricate ideal microwave-absorbing materials, conductive polymers, carbon materials and inorganic compounds are currently combined via chemical reaction. Liu and co-workers[7] fabricated graphene/poly(3,4-ethylenedioxythiophene)/Fe_3O_4 composites with uniform structure that displayed excellent microwave-absorbing properties, including a minimum reflection loss of − 56.5 dB at a frequency of 8.9 GHz. In addition, He et al.[8] designed a PANI/Ag/$SrFe_{12}O_{19}$ composite with superior microwave-absorbing properties and its minimum reflection loss value can reach − 14.86 dB in the X band.

Conductive polymers have special long conjugated structures, low density, good conductivity and many other advantages, and they are frequently used in the preparation of absorbing materials. The commonly used conductive polymers include polypyrrole (PPY), polyaniline (PANI) and polythiophene (PHT).[9–11] As a universal conducting polymer, PANI has many useful merits, which include its high

(Received February 2, 2018; accepted June 14, 2018; published online June 28, 2018)

conductivity, low weight and low cost.[12] Tian and coworkers[13] constructed a uniform core–shell PPy@PANI composite microsphere with tunable shell thickness, and when the material was applied as a microwave absorber, its reflection loss value could reach − 34.8 dB. In addition, many other PANI composites, including PANI/Ni/CF,[14] PANI/$NiFe_2O_4$/graphite nanosheet,[15] PANI/$SrFe_{12}O_{19}$/hollow glass beads,[16] have also been prepared by other researchers.

Metallic oxide with excellent dielectric properties, such as titanium dioxide and manganese dioxide, have regularly been chosen to prepare electromagnetic absorbing materials.[17–19] These materials are beneficial to the electrical loss of electromagnetic waves, and thereby promote absorption efficiency. She et al.[20] synthesized a spindle-type hollow polydopamine@α-MnO_2 with tunable microwave absorption frequency. Zhou et al.[21] designed a hollow urchin-like α-MnO_2 as a microwave absorption material, and its reflection loss can reach − 41 dB. As another perfect microwave absorber, Cheng and coworkers reported the facile preparation of TiO_2/$NiFe_2O_4$/hollow glass bead composites.[22]

In this work, a novel microwave absorber with low density and strong capacity was designed. First, MnO_2/CF was obtained through the oxidation–reduction reaction of mineral chameleon ($KMnO_4$) and carbon fiber. The nano-size MnO_2 particles were grown on the surface of CF *in situ*. Then, the binary hybrid was coated with the conductive polymer PANI via the suspension polymerization of aniline monomer in aqueous phase, which was initiated by ammonium persulfate. The microwave-absorbing properties of PANI, PANI/CF and PANI/MnO_2/CF hybrid were systematically evaluated. The PANI/MnO_2/CF hybrid was found to exhibit strong electromagnetic wave absorption capacity.[23–25]

EXPERIMENTAL

Synthesis of the MnO_2/CF

First, 100 mg of CF was uniformly dispersed in 80 mL of $KMnO_4$ solution (0.1 mol L^{-1}) by 30 min of vigorous ultrasonic treatment, and the suspension was transferred into a Teflon-lined stainless steel autoclave with a capacity of 100 mL. Then, the autoclave was sealed and kept at 150°C in an air-blast oven for about 90 min. Finally, when the temperature of the mixed reaction liquid had reached room temperature, the obtained brown precipitate was collected by filtration, washed several times using absolute ethyl alcohol and dried at 65°C for 8 h. The chemical reaction between $KMnO_4$ and CF in aqueous solution is assumed to obey the following equation[26]:

$$4KMnO_4 + 3C + H_2O \xrightarrow{150^\circ C} 4MnO_2 \downarrow + K_2CO_3 + 2KHCO_3 \quad (1)$$

Synthesis of the PANI/MnO_2/CF

The PANI/MnO_2/CF hybrid was synthesized by a simple *in situ* growth reaction of aniline monomer on the surface of MnO_2/CF. Briefly, 0.1 g of MnO_2/CF was dispersed uniformly in 30 ml of HCl solution (0.5 mol L^{-1}), and the emulsion was placed in an ice water bath and stirred for about 30 min. Then, 50 μL of aniline monomer was added dropwise to the suspension. When the temperature of the reaction system was maintain at about 0°C, 30 ml another mixed solution was slowly dropped into the suspension, which contains 0.5 mol L^{-1} ammonium persulfate and 0.5 mol L^{-1} HCl. The entire reaction was maintained at 0°C for about 300 min. Finally, the precipitate was collected by centrifuge (10000 r min^{-1}), washed with HCl solution (0.5 mol L^{-1}) several times and dried at 65°C for 12 h. The entire process diagram for the synthesis of PANI/MnO_2/CF hybrid is briefly illustrated in Fig. 1.[27]

Characterization

The surface structure of the samples was examined by scanning electron microscopy (SEM; JEOL JSM-6390, Tokyo, Japan). The chemical composition and crystalline phase of the samples were examined by x-ray powder diffraction (XRD, PANalytical, Netherlands). X-ray photoelectron spectroscopy (XPS; Thermo Scientific K-Alpha, Thermo Fisher, Waltham, MA, USA) was adopted to identify the elements and binding energy of PANI/MnO_2/CF. The functional groups of PANI-based materials were analyzed via Fourier transform infrared spectroscopy (FT-IR; WQF-310, Beijing Rayleigh Analytical Instrument Corporation, China). The thermal stabilities were measured using a thermogravimetric (TG) analyzer (SDT-2960, TA Instruments, USA) with a heating rate of 10°C/min in the range of 40°C to 800°C under an argon atmosphere. Relative complex permeabilities and permittivities of PANI, PANI/CF and PANI/MnO_2/CF were measured via an Agilent E8362B vector network analyzer in the X-band. The sample (20 wt.%) was bound to paraffin (80 wt.%), pressed and cured in a 22.86 mm × 10.16 mm × 2.0 mm mold, and the microwave absorption properties were subsequently evaluated by the calculated reflection loss (R_L) curves.[28–30]

RESULTS AND DISCUSSION

SEM Analysis

Figure 2 shows the SEM images derived from CF (a), MnO_2/CF (b and c) and PANI/MnO_2/CF (d). Figure 2a confirms that the surface of selected carbon fiber is smooth and glossy with an average diameter of about 6–7 μm. After the oxidation–

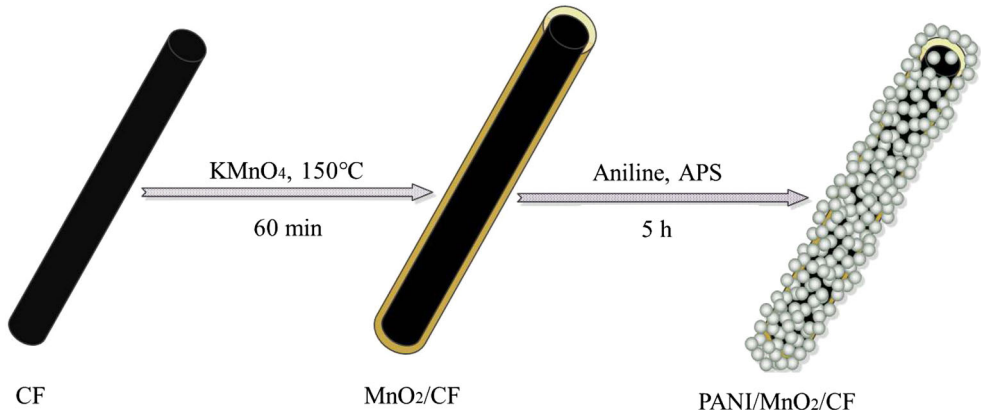

Fig. 1. Preparation process diagram of PANI/MnO_2/CF hybrid.

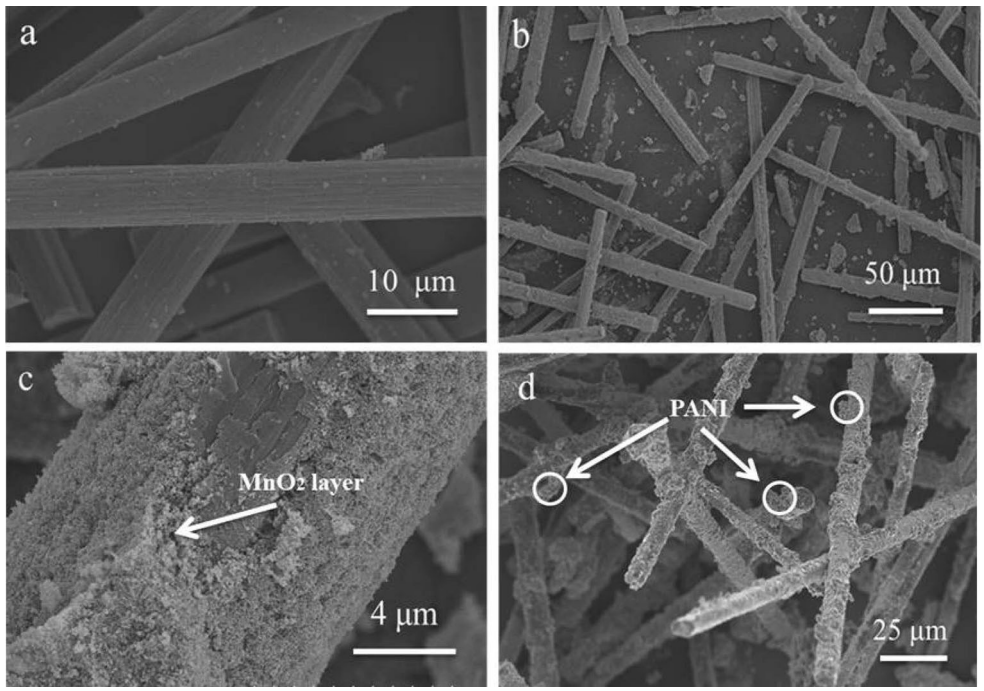

Fig. 2. SEM images for CF (a), MnO_2/CF (b, c), and PANI/MnO_2/CF (d).

reduction reaction, a large number of MnO_2 nano particles were produced and deposited on the surface of carbon fiber, and a uniform MnO_2 layer was formed, which is clearly observed in Fig. 2b and c. This is mainly due to the oxidation–reduction reaction of elemental carbon and $KMnO_4$. From Fig. 2c, the size of the synthesized MnO_2 particle is less than 50 nm. Figure 2d reveals the uniform morphology of the PANI/MnO_2/CF hybrid, which indicates that the MnO_2/CF was uniformly coated by another material and an original ternary hybrid was successfully prepared. The constituents of the products are labeled in Fig. 2c and d.

XRD Analysis

Figure 3 shows the XRD patterns for CF (a), MnO_2/CF (b) and PANI/MnO_2/CF (c). Crystal structures and components can be discussed using the patterns. In Fig. 3a and b, a very board diffraction peak centered at about 25° is evident, which indicates the poor crystallinity of carbon fiber. Compared with the patterns in Fig. 3a, the patterns in Fig. 3b display three additional characteristic peaks located at 37.52°, 41.97° and 65.11°, which indexes to the diffractions of (2 1 1), (3 0 1) and (0 0 2) planes of MnO_2 grain, respectively (JCPDS, No.44e0141). The emergence of these three characteristic peaks

illustrates the preparation of MnO_2/CF. The 3 sharp peaks located at 2θ = 14.9°, 20.1° and 25.2° are the characteristic peaks of protonic acid doped PANI. Compared with the XRD patterns of CF and MnO_2/CF, the diffraction peaks of PANI appear in the pattern shown in Fig. 3c, which proves that the cladding material is PANI, and the PANI/MnO_2/CF ternary hybrid was successfully fabricated.

XPS Analysis

The elemental composition of PANI/MnO_2/CF was measured using XPS, and the results are displayed in Fig. 4. In Fig. 4a, the wide scan XPS spectrum is observed, which confirms that the obtained reaction product consists of four elements, C, N, O and Mn. Figure 4b shows the narrow sweep spectrum for C1*s*. It can be divided into two peaks located at 284.6 eV and 285.3 eV, corresponding to C–C/C=C and C–N bonds, respectively. Figure 4c shows the narrow sweep spectrum of the N1*s*. It can divided into three peaks, which represent three different valence states of nitrogen in the PANI molecular chain, –N = , –NH– and –N+–. Figure 4d displays the narrow scan pattern for oxygen. The binding energy peaks at 530.0 eV and 531.6 eV are assigned to O-Mn and O–H, respectively. In Fig. 4e, the presence of the two peaks at 641.8 eV and 652.1 eV can be attributed to the Mn2$p_{3/2}$ and Mn2$p_{1/2}$ binging energy, respectively. In addition, the Mn3*p* characteristic peak and Mn3*s* characteristic peak can also be observed in the wide scan spectrum. Based on the above analysis, the PANI/MnO_2/CF hybrid was fabricated, and the conclusion is consistent with the previous results of SEM and XRD analysis.[31–33]

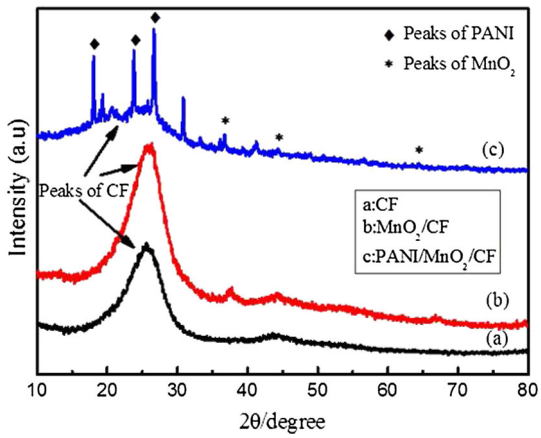

Fig. 3. XRD patterns of CF (a), MnO_2/CF (b), and PANI/MnO_2/CF (c).

FT-IR Analysis

The functional groups of PANI(a), PANI/CF(b) and the PANI/MnO_2/CF(c) hybrid were investigated via FT-IR, and their patterns are displayed in Fig. 5. From the patterns, all three of the analyzed samples possess peaks characteristic of PANI located at 1559 cm^{-1}, 1477 cm^{-1}, 1259 cm^{-1}, 1155 cm^{-1} and 797 cm^{-1}, respectively, which has

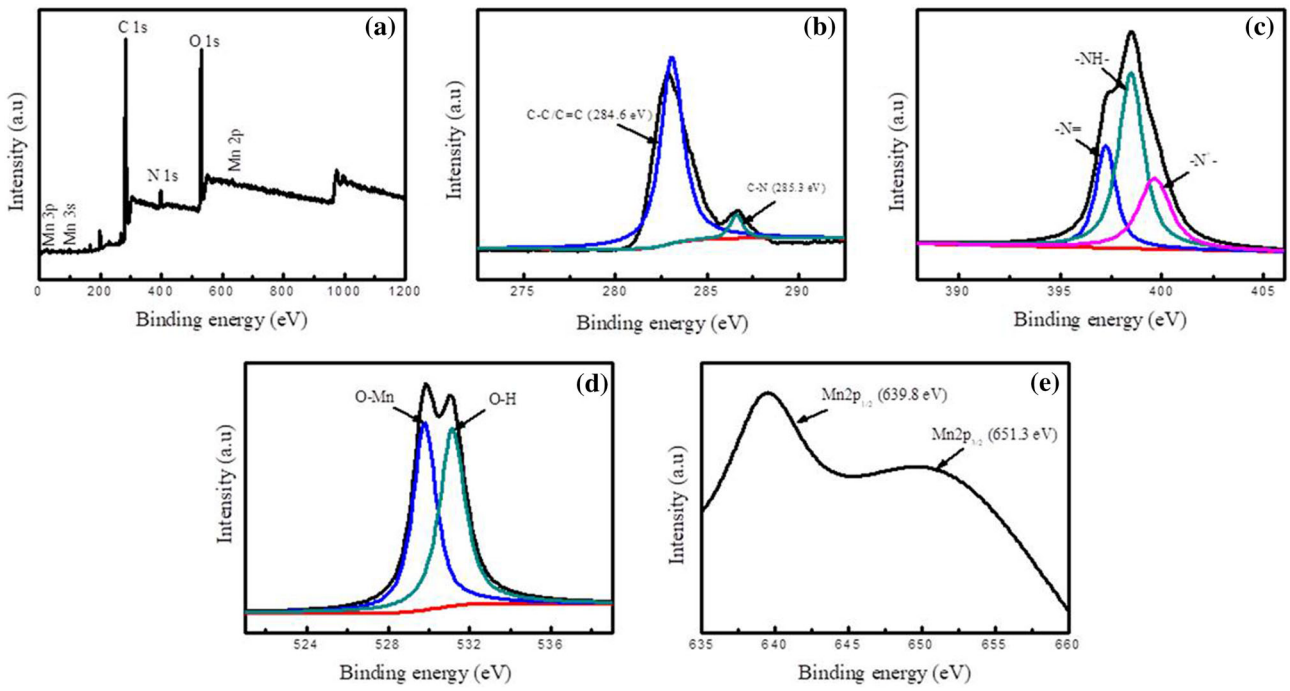

Fig. 4. Wide scan (a), C1*s* (b), N1*s* (c), O1*s* (d), and Mn2*p* (e) spectrum of PANI/MnO_2/CF.

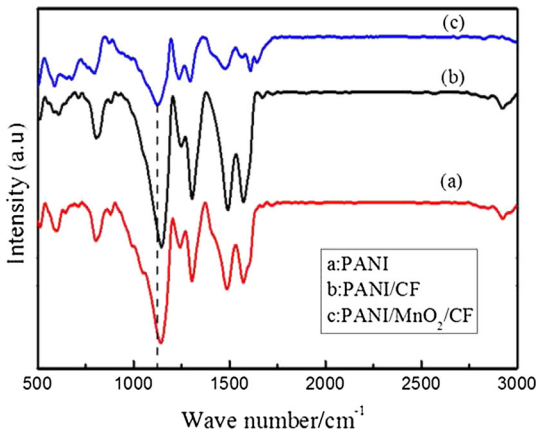

Fig. 5. FT-IR spectra of PANI (a), PANI/CF (b), and PANI/MnO_2/CF (c).

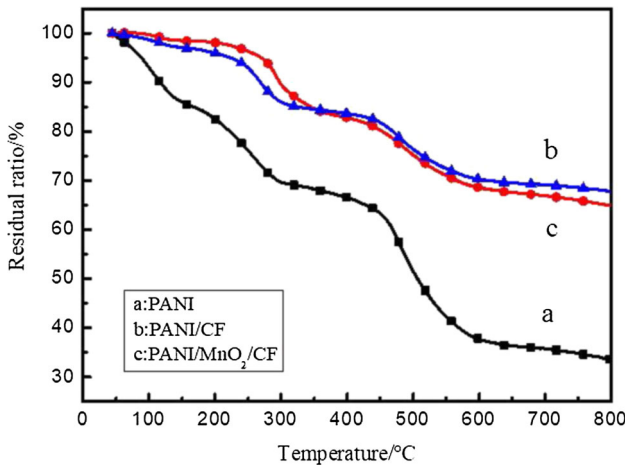

Fig. 6. TG curves of PANI (a), PANI/CF (b), and PANI/MnO_2/CF (c).

been reported in the literature previously.[34] The characteristic peaks located at 1559 cm^{-1} and 1477 cm^{-1} can primarily be attributed to the C–C and C=C stretching vibration of the benzenoid ring of the PANI backbone. The peak located at 1259 cm^{-1} corresponds to C–N stretching of the backbone of PANI. The peak at 1155 cm^{-1} is assigned to the quinonoid ring of PANI, and the peak located at 797 cm^{-1} is due to the flexural oscillation of the out-of-plane deformation of C–H in the p-disubstituted benzene ring.[35] These values are consistent with those of previous studies. Compared with PANI, some of the characteristic peaks (e.g. the peak located at 1155 cm^{-1}) of PANI/CF and PANI/MnO_2/CF exhibit a significant blueshift (from the lower wave numbers to the higher wave numbers), which may be due to the addition of carbon fiber.[36]

TG Analysis

Heat endurance is an important performance criterion for subsequent application of the prepared materials. Therefore, TG analysis was adopted to measure the thermal stability of PANI, PANI/CF and PANI/MnO_2/CF, and their thermogravimetric curves are shown in Fig. 6. The degradation temperature (50% residual ratio) of PANI is about 500°C, and degradation occurs due to the pyrolysis of its macromolecular backbone. The TG curves of the PANI/CF and PANI/MnO_2/CF are very similar. However, all the corresponding residual ratios of the PANI are lower than that of PANI/CF and PANI/MnO_2/CF, which indicates the heat endurance of PANI/CF and PANI/MnO_2/CF is superior to that of PANI. When the temperature approached 800°C, the residual ratio of PANI, PANI/CF and PANI/MnO_2/CF was 33%, 67% and 70%, respectively. The promotion of heat resistance can be attributed to the role of CF in imposing restriction on the pyrolysis of PANI chains and avoiding heat concentration.[37,38] Compared with polyaniline, PANI/MnO_2/CF is more suitable for use as a thermally stable microwave-absorbing material.

Microwave-Absorbing Performance Analysis

In general, electromagnetic waves incident on any media will be reflected and transmitted (absorbed by absorbing material) by the media. Waves in the form of electromagnetic energy can be fully or partially absorbed and dissipated into the absorbing materials through magnetic and dielectric losses. The absorbed energy is transformed into heat, which gives rise to electromagnetic losses. Since microwaves have electric and magnetic components, the absorption mechanism of a material can be divided into dielectric loss and magnetic loss, which can measured by ε', ε'', μ' and μ''. ε', where μ' is correlated with the storage capability, while ε'' and μ'' represent the dissipation capability of electric and magnetic energy, respectively.[39,40] The R_L curves of materials can be calculated by using ε', ε'', μ' and μ'', and the relevant equations are as follows[41–43]:

$$\Gamma = \frac{Z_{in} - Z_0}{Z_{in} + Z_0} \tag{2}$$

$$Z_0 = (\mu_0/\varepsilon_0)^{1/2} \tag{3}$$

$$Z_{in} = Z_0\left(\sqrt{\frac{\mu_r}{\varepsilon_r}}\right)\tanh\left[j\left(\frac{2\pi fd}{c}\right)\left(\sqrt{\mu_r\varepsilon_r}\right)\right] \tag{4}$$

$$R_L = 20\log\left(\frac{Z_{in} - Z_0}{Z_{in} + Z_0}\right) \tag{5}$$

where Z_0 stands for the impedance of the free space, Z_{in} is the input impedance of the absorber, $\mu_r = \mu' - j\mu''$ is the relative permeability, $\varepsilon_r = \varepsilon' - j\varepsilon''$ is the relative permittivity, f is the frequency of the incident microwave, t is the thickness of the absorber and c is the velocity of light in free space.[43]

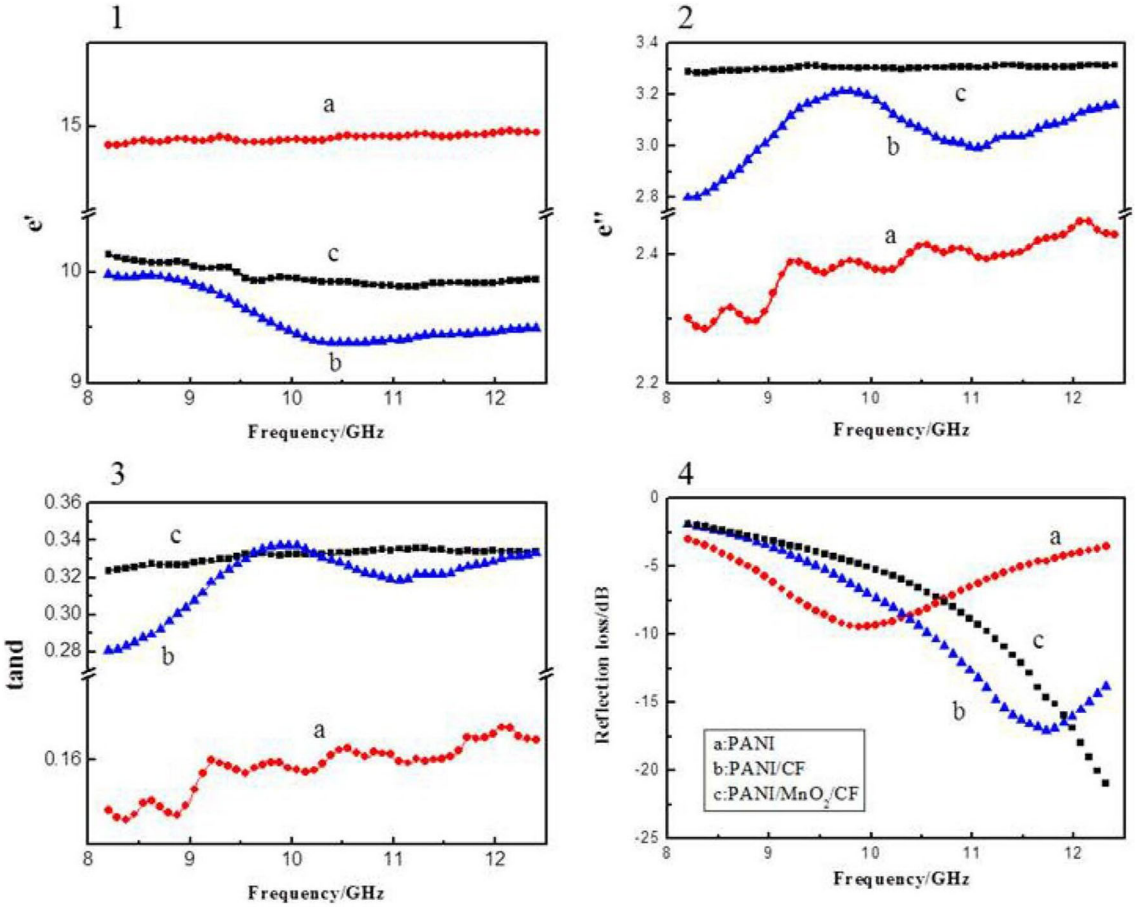

Fig. 7. The dielectric properties (1, 2, 3) and R_L curves (4) of PANI (a), PANI/CF (b), and PANI/MnO_2/CF (c).

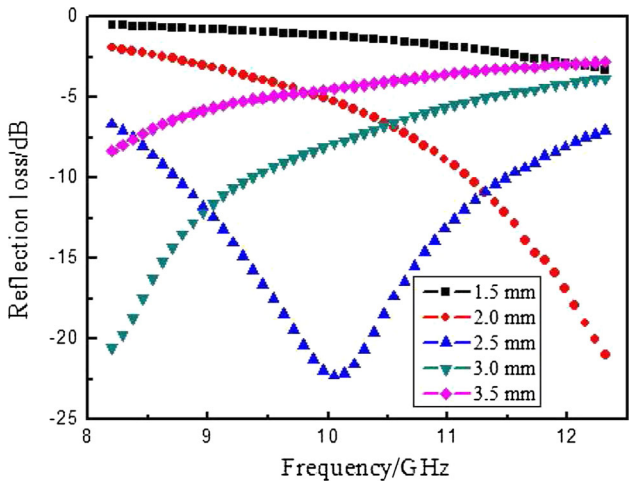

Fig. 8. R_L curves of PANI/MnO_2/CF at different thicknesses.

Therefore, the thickness of the sample has a significant influence on its microwave-absorbing properties. Consequently, CF, PANI and MnO_2 all perform as non-magnetism materials. The magnetic parameters μ' and μ'' of the PANI, PANI/CF and PANI/MnO_2/CF hybrid are 1 and 0, respectively.[44,45]

Dielectric loss derived from the relaxation processes is vital for the mechanism of absorption for electromagnetic waves. The permittivities of the samples are shown in Fig. 7-1 and 7-2. Additionally, their dielectric loss (tan $\delta_e = \varepsilon''/\varepsilon'$) was calculated and is shown in Fig. 7-3. In the X band, the real part, imaginary part and tan δ_e values of PANI/CF (b) and PANI/MnO_2/CF (c) are fairly similar, and they are significantly higher than that of PANI (a). This is mainly due to the excellent electrical conductivity of PANI/CF and PANI/MnO_2/CF. The calculated frequency dependence R_L curves of PANI, PANI/CF and PANI/MnO_2/CF are shown in Fig. 7-4. The R_L value of PANI in the X band was less than − 10 dB (90% absorption), from − 2.5 dB, to − 9 dB, which indicates the sample's microwave absorption performance is poor. When combined with CF, the absorption performance was improved. The lowest value of the R_L curves can reach − 17 dB. Furthermore, the R_L curve of the PANI/MnO_2/CF was below the R_L curve of PANI, and its lowest frequency appears at F = 12.4 GHz, with a value of about − 22 dB (more than 99% absorption). When the frequency ranged from 11.0 GHz to 12.4 GHz, its R_L values were all less than − 10 dB. These results illustrate that the microwave-absorbing properties

of the PANI/MnO_2/CF hybrid were greatly improved relative to PANI, and they were also better than those of PANI/CF, which is mainly due to the combination of three components: PANI, CF and MnO_2. The conductivity was increased and the dielectric loss was enhanced, therefore, better electromagnetic wave-absorbing performance is observed.[46–48]

On the basis of Eqs. 2, 3, 4 and 5, the thickness of the material has a significant influence on the peak position and intensity of its R_L curves, which is related to the quarter-wavelength matching model. Thus, it is necessary to simulate the electromagnetic wave absorption properties of the sample based on its thickness. The simulated R_L curves depending on the thickness of the PANI/MnO_2/CF hybrid are displayed in Fig. 8. It is apparent that the thickness of the absorber has a remarkable influence on the electromagnetic wave-absorbing properties. The minimum R_L gradually shifts toward lower frequency with an increase of thickness, which agrees with the quarter-wavelength model. When the thickness reached 2.5 mm, the PANI/MnO_2/CF sample exhibited the best microwave-absorbing capacity. As the thickness deviates from 2.5 mm, the microwave absorption becomes weaker. When the thickness is 2.5 mm, the R_L value of the sample can approach − 23 dB at 10.2 GHz. When the frequency ranges from 8.7 GHz to 11.7 GHz, the R_L values are all less than − 10 dB, which means that the effective absorption bandwidth is 3.0 GHz. Therefore, in the X band, the best matching thickness of the PANI/MnO_2/CF hybrid is 2.5 mm.[49–51]

CONCLUSIONS

2In summary, a uniform PANI/MnO_2/CF hybrid with superior microwave absorption properties can be prepared via a simple two-step reaction involving the oxidation–reduction reaction of CF and $KMnO_4$ and *in situ* polymerization of polyaniline. Due to the enhancement in dielectric loss, the microwave-absorbing capacity of PANI/MnO_2/CF was greater than that of PANI and PANI/CF, and its minimum loss value can reach − 22 dB at 10.2 GHz. When the frequency ranges from 8.7 GHz to 11.7 GHz, the R_L values are all less than − 10 dB, which implies that the effective absorption bandwidth can reach 3.0 GHz in the X band. In view of the results presented herein, the PANI/MnO_2/CF hybrid can be regarded as an ideal microwave absorber.

ACKNOWLEDGEMENTS

The authors are grateful for the support and funding provided by the Foundation of National Natural Science Foundation of China (No. 51773169); Space Supporting Fund from China Aerospace Science and Industry Corporation (No. 2017-HT-XG); and the Fundamental Research Funds for the Central Universities (No. 3102017jg02003).

REFERENCES

1. Y.C. Qing, Q.L. Wen, F. Luo, W.C. Zhou, and D.M. Zhu, *J. Mater. Chem. C.* 4, 371 (2016).
2. M. Cao, W. Song, Z. Hou, B. Wen, and J. Yuan, *Carbon* 48, 788 (2010).
3. T.K. Gupta, B.P. Singh, R.B. Mathur, and S.R. Dhakate, *Nanoscale* 6, 842 (2014).
4. S. Yang, X. Cui, J. Gong, and Y. Deng, *Chem. Commun.* 49, 4676 (2013).
5. A.L. Feng, Z.R. Jia, Y. Zhao, and H.L. Lv, *J. Alloys Compd.* 745, 547 (2018).
6. G.L. Wu, Y.H. Cheng, Z.H. Yang, Z.R. Jia, H.J. Wu, L.J. Yang, H.L. Li, P.Z. Guo, and H.L. Lv, *Chem. Eng. J.* 333, 519 (2018).
7. P.B. Liu, Y. Huang, and X. Zhang, *J. Alloys Compd.* 617, 511 (2014).
8. Z. He, S.H. Qi, X.L. Zhong, H. Ma, P. Wang, and H. Qiu, *J. Alloys Compd.* 621, 194 (2015).
9. J. Xu, K. Wang, S. Zu, B. Han, and Z. Wei, *ACS Nano* 4, 5019 (2010).
10. Y. Yang, S. Qi, and X. Zhang, *Mater. Lett.* 66, 229 (2012).
11. X.B. Fan, W.C. Peng, Y. Li, X.Y. Li, S.L. Wang, G.L. Zhang, and F.G. Zhang, *Adv. Mater.* 20, 4490 (2008).
12. G.A. Snook, P. Kao, and A.S. Best, *J. Power Sour.* 196, 1 (2011).
13. C.H. Tian, Y.C. Du, P. Xu, R. Qiang, Y. Wang, D. Ding, J.L. Xue, J. Ma, H.T. Zhao, and X.J. Han, *ACS Appl. Mater. Interfaces* 7, 20090 (2015).
14. X.L. Chen, X.W. Wang, L.D. Li, and S.H. Qi, *J. Mater. Sci.: Mater. Electron.* 27, 5607 (2016).
15. L. Sun, Q. Li, W. Wang, J. Pang, and J. Zhai, *Appl. Surf. Sci.* 257, 10218 (2011).
16. X.L. Chen and S.H. Qi, *J. Sol-Gel. Sci. Technol.* 81, 824 (2017).
17. J. Jiang, L. Li, and F. Xu, *J. Phys. Chem. Solids* 68, 1656 (2007).
18. Y. Meng, K. Wang, Y. Zhang, and Z. Zhang, *Adv. Mater.* 25, 6985 (2013).
19. J. Yang, Y.Z. Zhou, L. Sun, N. Zhao, C.L. Zang, and X.N. Cheng, *Appl. Surf. Sci.* 258, 5056 (2012).
20. W. She, H. Bi, Z.W. Wen, Q.H. Liu, X.B. Zhao, J. Zhang, and R.C. Che, *ACS Appl. Mater. Interfaces* 8, 9782 (2016).
21. M. Zhou, X. Zhang, J.M. Wei, S.L. Zhao, L. Wang, and B.X. Feng, *J. Phys. Chem. C* 115, 1398 (2011).
22. C. Shi, J. Zhu, X. Shen, F. Chen, F. Ning, H. Zhang, Y. Long, X. Ning, and J. Zhao, *RSC Adv.* 8, 4072 (2018).
23. S. Kim, S. Zhou, Y.K. Hu, M. Acik, Y.J. Chabal, C. Berger, W.D. Heer, and E. Riedo, *Nat. Mater.* 11, 544 (2012).
24. A. Feng, G. Wu, C. Pan, and Y. Wang, *J. Nanosci. Nanotechnol.* 17, 3786 (2017).
25. G.L. Wu, H.J. Wu, K.K. Wang, C.H. Zheng, Y.Q. Wang, and A.L. Feng, *RSC Adv.* 6, 58069 (2016).
26. J. Yu, N. Grossiord, C.E. Koning, and J. Loos, *Carbon* 45, 618 (2007).
27. X.L. Chen, X.W. Wang, L.D. Li, and S.H. Qi, *J. Mater. Sci.: Mater. Electron.* 27, 10045 (2016).
28. H. Wu, G. Wu, Y. Ren, X.H. Li, and L.D. Wang, *Chem. A Eur. J.* 22, 8864 (2016).
29. A. Feng, G. Wu, C. Pan, and Y. Wang, *J. Nanosci. Nanotechnol.* 17, 3859 (2017).
30. Q. Liu, Z. Zi, M. Zhang, P. Zhang, A. Pang, J. Dai, and Y. Sun, *J. Mater. Sci.* 48, 6048 (2013).
31. T.H. Ting, R.P. Yu, and Y.N. Jau, *Mater. Chem. Phys.* 126, 364 (2011).
32. G. Wu, K. Kou, N. Li, and M. Chao, *J. Appl. Polym. Sci.* 128, 1164 (2013).
33. A.L. Feng, Z.R. Jia, Q. Yu, H.X. Zhang, and G.L. Wu, *NANO* 13, 1850037 (2018).
34. Y. Wang, K. Kou, G. Wu, L. Zhuo, J. Li, and Y. Zhang, *Polymer* 77, 354 (2015).
35. Y.C. Qing, Q.L. Wen, F. Luo, W.C. Zhou, and D.M. Zhu, *J. Mater. Chem. C.* 4, 371 (2016).

36. B. Kaur, M. Bhat, F. Licci, R. Kumar, and S.D. Kulkarni, *J. Magn. Magn. Mater.* 305, 392 (2006).
37. Y. Xie, X. Hong, X. Wang, J. Zhao, Y. Gao, and Y. Ling, *Synth. Met.* 162, 1643 (2012).
38. W. Jing, Z. Hong, B. Shuxin, C. Ke, and Z. Changrui, *J. Magn. Magn. Mater.* 312, 310 (2007).
39. D. Chen, G. Wang, S. He, J. Liu, L. Guo, and M. Cao, *J. Mater. Chem. A.* 1, 5996 (2013).
40. X.L. Chen and S.H. Qi, *J. Mater. Sci.: Mater. Electron.* 27, 13099 (2016).
41. H. Lv, Y. Guo, G. Wu, G. Ji, Y. Zhao, and Z.J. Xu, *ACS Appl. Mater. Interfaces* 9, 5660 (2017).
42. H. Zengin, W. Zhou, J. Jin, R. Czerw, D.W. Smith, L. Echegoyen, D.L. Carroll, S.H. Foulger, and J. Ballato, *Adv. Mater.* 14, 1480 (2002).
43. Y. Chen, B. Song, X. Tang, L. Lu, and J. Xue, *Small* 10, 1536 (2014).
44. M.S. Cao, J. Yang, W.-L. Song, D.Q. Zhang, B. Wen, H.B. Jin, Z.L. Hou, and J. Yuan, *ACS Appl. Mater. Interfaces* 4, 6949 (2012).
45. G. Sun, B. Dong, M. Cao, B. Wei, and C. Hu, *Chem. Mater.* 23, 1587 (2011).
46. H. Lv, Z. Yang, P. Wang, G. Ji, J. Song, L. Zheng, H. Zeng, and Z.J. Xu, *Adv. Mater.* 30, 1706343 (2018).
47. J. Liu, R. Che, H. Chen, F. Zhang, F. Xia, Q. Wu, and M. Wang, *Small* 8, 1214 (2012).
48. H. Wu, Y. Wang, C. Zheng, J. Zhu, G. Wu, and X. Li, *J. Alloys Compd.* 685, 8 (2016).
49. J. Liu, J. Xu, R. Che, H. Chen, Z. Liu, and F. Xia, *J. Mater. Chem.* 22, 9277 (2012).
50. J. Yan, Z. Fan, T. Wei, W. Qian, M. Zhang, and F. Wei, *Carbon* 48, 3825 (2010).
51. X. Guo, Y. Deng, D. Gu, R. Che, and D. Zhao, *J. Mater. Chem.* 19, 6706 (2009).